催 化 学 报
2012 Chinese Journal of Catalysis Vol. 33 No. 9

文章编号: 0253-9837(2012)09-1523-09 国际版 DOI: 10.1016/S1872-2067(11)60427-0 研究论文: 1523–1531

WO_3 改性方法对 MnO_x/TiO_2 催化剂低温催化 NH_3 还原 NO 特性的影响

张亚平, 汪小蕾, 沈 凯*, 徐海涛, 孙克勤, 周长城

东南大学能源与环境学院, 能源热转换及其过程测控教育部重点实验室, 江苏南京 210096

摘要: 采用 3 种不同的浸渍过程制备了系列 WO_3 改性 MnO_x/TiO_2 催化剂, 并采用 BET 比表面积测试、X 射线衍射、拉曼光谱、H_2 程序升温还原、高分辨扫描电镜和原位红外光谱等技术进行表征. 结果显示, 一步浸渍法和先钨后锰的分布浸渍法制备的催化剂中, Mn 和 W 的协同作用提高了活性组分的分散状态, 并阻止了钛载体的转晶; 在所有的 Mn 基催化剂中, Mn 物种主要以 Mn_2O_3 形式存在, 但在 15%MnO_x-5%WO_3/TiO_2 中出现了少量的 MnO_2; WO_3 的加入大大增强了催化剂的还原能力, 提高了其表面酸位尤其是 B 酸的数量与强度, 并促进了活性中间物 ($-NH_2$) 的生成. 表面 Lewis 酸在低温 SCR 反应起主要作用, 并且发现 $-NH_2$ 也是活性很高的物种. 在 NH_3 低温催化还原 NO 的反应中, 一步浸渍法制备的催化剂活性最高.

关键词: 钨氧化物; 改性; 锰氧化物; 低温选择性催化剂还原; 表面酸位; 活性中间产物

中图分类号: O643 **文献标识码**: A

收稿日期: 2012-05-15. 接受日期: 2012-06-21.

*通讯联系人. 电话: (025)83790771; 传真: (025)83791033; 电子信箱: amflora@seu.edu.cn

基金来源: 国家高技术研究发展计划 (863 计划, 2007AA061802); 江苏省自然科学基金重点项目 (BK2008001).

本文的英文电子版(国际版)由Elsevier出版社在ScienceDirect上出版(http://www.sciencedirect.com/science/journal/18722067).

WO_3 Modification of MnO_x/TiO_2 Catalysts for Low Temperature Selective Catalytic Reduction of NO with Ammonia

ZHANG Yaping, WANG Xiaolei, SHEN Kai*, XU Haitao, SUN Keqin, ZHOU Changcheng

Key Laboratory of Energy Thermal Conversion and Control of Ministry of Education, School of Energy and Environment, Southeast University, Nanjing 210096, Jiangsu, China

Abstract: A series of WO_3-modified MnO_x/TiO_2 catalysts were prepared by three different impregnation methods and were investigated by specific surface area measurement, X-ray diffraction, laser Raman spectroscopy, H_2 temperature-programmed reduction, high-resolution transmission electron microscopy, and in situ Fourier transform infrared spectroscopy. The three-component catalysts obtained with the one-step impregnation exhibited the best catalytic activity. The characterization data revealed that a synergism between tungsten and manganese oxide existed in the catalysts when tungsten was loaded either prior to or simultaneously with manganese, which made the active components better dispersed and blocked the transformation of TiO_2 from the anatase to rutile structure. The manganese oxide existed in the form of Mn_2O_3 on all the samples but was accompanied by a small amount of MnO_2 for 15%MnO_x-5%WO_3/TiO_2. WO_3 improved the reducibility and enhanced the amount and strength of the surface acid sites, especially the Brönsted acid sites and promoted the formation of the active intermediate ($-NH_2$). Lewis acid sites had the major role in the low temperature selective catalytic reduction reaction while surface $-NH_2$ was an important intermediate species.

Key words: tungsten oxide; modification; manganese oxide; low-temperature selective catalytic reduction; surface acidity; active intermediate

Received 15 May 2012. Accepted 21 June 2012.

**Corresponding author. Tel: +86-25-83790771; Fax: +86-25-83791033; E-mail: amflora@seu.edu.cn*

This work was supported by the National High Technology Research and Development Program of China (863 Program, 2007AA061802) and the Natural Science Foundation of Jiangsu Province (BK2008001).

English edition available online at Elsevier ScienceDirect (http://www.sciencedirect.com/science/journal/18722067).

There is interest in developing a low temperature (353–533 K) selective catalytic reduction (SCR) catalyst so that the catalyst bed can be placed downstream of the desulfurization scrubber and/or particulate control device where most of sulfur dioxide and dust is removed to have less deactivation. Some transition metal containing catalysts, including Cr/TiO_2 [1], $NiSO_4/Al_2O_3$ [2], MnO_x/Al_2O_3 [3], V_2O_5/activated carbon [4], CuO/Al_2O_3 [5], CuO/TiO_2 [6], Fe_2O_3/TiO_2 [7], iron-silica aerogels [8], MnO_x/NaY [9], and other oxides [10], had been investigated and shown to be active for medium temperature SCR of NO with NH_3 in the presence of excess oxygen. Peña et al. [11] investigated a series of catalysts prepared from various transition metal oxides (V, Cr, Mn, Fe, Co, Ni, and Cu) on titania and reported that MnO_x/TiO_2 catalysts can be used below 423 K with both high NO conversion and N_2 selectivity.

Manganese oxide has attracted interest for its higher SCR activity at low temperature. It contains various types of labile oxygen, which are necessary in the catalytic cycle [12]. Mn-based low temperature catalysts that have been investigated can be divided into three categories: unsupported, supported, and binary metal oxide-based catalysts. The activity and selectivity of pure manganese oxide in SCR was investigated by Kapteijn et al. [12], and 90% NO conversion was obtained at 450 K. For the supported catalysts, carriers like Al_2O_3 [3], TiO_2 [13,14], USY [15], MnO_x/AC [16], and MnO_x/ACF [17] have been widely studied. Among these, MnO_x/TiO_2 catalysts gave a higher catalytic activity at low temperature [11]. The other kind of Mn-based catalysts are mixed oxides doped with a transitional metal to make use of a synergistic effect between the two metal oxides. Mn-Fe composite oxides have been investigated. Chen et al. [18] reported that a Fe(0.4)-MnO_x catalyst showed the best activity, yielding 98.8% NO_x conversion and 100% selectivity for N_2 at 393 K and a space velocity of 30000 h^{-1}. This may be due to the formation of the active center $Fe_3Mn_3O_8$. Liu et al. [19] reported that the interaction of iron, manganese, and titanium species in $Fe_{0.5}Mn_{0.5}TiO_2$ catalyst gave the highest SCR activity. Some researchers have suggested that adding other metal oxides into MnO_x/TiO_2 can give it a higher low temperature activity. For examples, Li et al. [20] prepared a series of Cr-Mn catalysts by co-precipitation and found that Cr(0.4)-MnO_x had a high low temperature SCR activity due to the formation of $CrMn_{1.5}O_4$. Wu et al. [21] studied the effect of various transition metals (Fe, Cu, Ni, and Cr) on the catalytic activity of a Mn/TiO_2 catalyst and reported that the ternary oxides exhibited better catalytic performance than the double oxide counterparts. In particular, Cu (0.1)-Mn(0.6)/TiO_2 and Cr(0.1)-Mn(0.6)/TiO_2 gave 95% NO reduction at 413 K and Ni(0.1)-Mn(0.6)/TiO_2 gave 99% conversion. In addition, the carrier-free Cr(0.4)-MnO_x catalyst prepared by Chen et al. [22] gave 98.5% NO conversion at 393 K. Wu et al. [23] investigated TiO_2-supported MnO_x catalysts doped with a second metal, e.g., Fe_2O_3, WO_3, MoO_3, and Cr_2O_3 and found that the catalytic performance at low temperatures decreased in the order of Mn-W/TiO_2 > Mn-Fe/TiO_2 > Mn-Cr/TiO_2 > Mn-Mo/TiO_2, but the N_2 selectivity decreased in the order of Mn-Fe/TiO_2 > Mn-W/TiO_2 > Mn-Mo/TiO_2 > Mn-Cr/ TiO_2. In our previous studies [24], it was also confirmed that Mo improved the catalytic activity and SO_2 resistance of MnO_x/TiO_2.

WO_3 is widely used as a promoter in the commercial V_2O_5-WO_3/TiO_2 catalyst. WO_3 provides high thermal stability to the catalyst by forming W–Ti–O chemical bonds on the TiO_2 surface [25], which inhibited the sintering of anatase TiO_2 and the anatase to rutile transition. In addition, WO_3 was reported to give a wider temperature window of SCR, increased the poison resistance to alkali metal oxides and arsenic oxide, and reduced ammonia oxidation and SO_2 oxidation [26]. With some SO_2 remaining even after the desulfurizer, both TiO_2 and WO_3 were more resistant to sulfur poisoning. Therefore, the ternary WO_3-MnO_x/TiO_2 catalyst can be a good catalyst for the low temperature SCR system.

In our previous report [27], the effect of WO_3 modification on a MnO_x/TiO_2 catalyst was studied. In this report, our research was focused on the comparative study of MnO_x-WO_3/TiO_2 catalysts synthesized by a one-step impregnation method with two different step-by-step preparation methods [27]. The catalysts were characterized by specific surface area measurement, X-ray diffraction (XRD), high-resolution transmission electron microscopy (HRTEM), laser Raman spectroscopy (LRS), H_2 temperature-programmed reduction (H_2-TPR), and in situ FT-IR.

1 Experimental

1.1 Preparation of catalysts

The MnO_x/TiO_2 samples were prepared by the impregnation of TiO_2 (Degussa, P25) with manganese acetate. The deionized water (50 ml) was added to an 80 ml beaker containing 2.0 g of TiO_2 with steady stirring. Then, the appropriate amount of manganese acetate precursor was added.

WO_3/TiO_2 catalysts were also prepared by impregnating the same titania support with a water solution of ammonium paratungstate and oxalic acid. $MnO_x/WO_3/TiO_2$ catalysts were synthesized by a step-by-step impregnation of WO_3/TiO_2 with the solution of manganese acetate. $WO_3/MnO_x/TiO_2$ catalyst was also prepared by the step-by-step impregnation of MnO_x/TiO_2 with a solution of ammonium paratungstate and oxalic acid. The MnO_x-WO_3/TiO_2 catalyst was prepared by a one-step impregnation method. The required amount of hydrated am-

monium paratungstate was added and dissolved in the solution of oxalic acid. Then, manganese acetate was added and the carrier titania was added to the mixture with continuously stirring. All the mixtures obtained after impregnation were stirred for 2 h at 25 °C and then at 85 °C for 4 h before they were dried overnight at 110 °C and calcined at 500 °C for 2 h. The loadings of MnO_x and WO_3 were 15 wt% and 5 wt%, respectively.

1.2 Catalytic activity

SCR activity measurements were carried out in a fixed bed reactor (i.d. 6 mm) at 80–300 °C containing 0.3 g of catalyst with a gas hourly space velocity (GHSV) of 24,000 h^{-1}. The total gas flow was 100 ml/min, which was premixed in a gas mixer to give the simulated gas of 0.08% of NO, 0.08% of NH_3, 5% of O_2, and balanced by N_2. Then the gas mixture was fed into the reactor. The NO and NO_2 concentrations were continuously monitored by a flue gas analyzer (Testo 330-2 LL).

1.3 Characterization of catalysts

Specific surface areas of the catalysts were measured by nitrogen adsorption at liquid N_2 temperature (−196 °C), using a Micromeritics F-sorb 3400 (Beijing Jinaipu, China) adsorption apparatus. An XD-3 diffractometer (Beijing PEPSEE, China) was employed with Cu K_α radiation (λ = 0.15406 nm) to get the XRD patterns of the catalysts. H_2-TPR was carried out in a quartz U-tube reactor connected to a thermal conduction detector (TCD) using a H_2-Ar mixture (7.3% H_2 by volume) as reductant. TPR was started from room temperature to 700 °C at a rate of 10 °C/min. Raman analysis was carried out on a Renishaw RM 2000 confocal microscope Raman spectrometer. A visible laser was used as the excitation light source with the following analysis parameters: output light intensity at 100% and 50%, scanning from 1200 to 100 cm^{-1} with a resolution of 1 cm^{-1}, the wavelength of the laser at 514.5 nm and the microscopic confocal area less than or equal to 1 μm.

The size and morphology of all the samples were measured with a JEM-2100 (JEOL, Japan) HRTEM. In situ FT-IR of ammonia adsorption was carried out on a Nicolet 5700 FT-IR instrument (Thermo Electron Corporation, USA) running at 4 cm^{-1} resolutions.

2 Results and discussion

2.1 Specific surface area

Table 1 presented the specific surface area of the different catalysts. It was 55.3 m^2/g for the original titania carrier, and it was decreased after Mn was loaded. Combined with the XRD results discussed later, which indicated that there was no crystalline manganese oxide on the surface, it can be inferred that amorphous MnO_x was dispersed on the surface of titania and occupied the pores, hence resulting in the decrease of surface area. For the sample with 5% of WO_3 loaded on the TiO_2 carrier, the specific surface area was 58.7 m^2/g. The result suggested that a low WO_3 loading can improve the structure of the carrier and increase the specific surface area as well.

Table 1 Specific surface area of the different catalysts

Sample	$A_{BET}/(m^2/g)$
TiO_2	55.3
$5\%WO_3/TiO_2$	58.7
$15\%MnO_x/TiO_2$	49.7
$15\%MnO_x/5\%WO_3/TiO_2$	52.3
$5\%WO_3/15\%MnO_x/TiO_2$	32.8
$15\%MnO_x$-$5\%WO_3/TiO_2$	50.8

The influence of the loading sequence of WO_3 on the tertiary oxides catalyst was also investigated. Of all he modified MnO_x/TiO_2 samples with 5% WO_3, the $15\%MnO_x/5\%WO_3/TiO_2$ sample possessed the largest specific surface area (52.3 m^2/g). The $15\%MnO_x$-$5\%WO_3/TiO_2$ sample exhibited a similar specific surface area (50.8 m^2/g), while for the $5\%WO_3/15\%MnO_x/TiO_2$ sample, the specific surface area decreased to 32.8 m^2/g, which was possibly due to the sintering of the metal oxide on the surface of MnO_x/TiO_2. This result showed the excellent thermal stability of the tungsten-modified carrier, WO_3/TiO_2.

2.2 XRD analysis

Figure 1 showed the XRD patterns of the different catalysts and carriers. Many peaks for anatase TiO_2 were observed while only a few peaks of rutile TiO_2 were detected for the carrier. With 15% MnO_x loading, the peaks corresponding to TiO_2 were still clearly observed but their intensities had decreased, which suggested that Mn had interacted with TiO_2 and covered the surface of TiO_2 [28]. However, for the 5% WO_3/TiO_2 sample, the intensity of the peak at 41.23° attributed to rutile TiO_2 was lower and even zero while the peaks for anatase TiO_2 were detected but were also weaker, as shown in Fig. 1(5). All WO_3-modified MnO_x/TiO_2 samples exhibited similar XRD patterns except that: (1) for the $15\%MnO_x/5\%WO_3/TiO_2$ sample, the strong characteristic peak for rutile titania at 27.5°, and the weak peaks at 36.08° and 41.23° were not observed, while the peak at 68.76° ascribed to anatase TiO_2 became almost zero, (2) for the other two WO_3-containing MnO_x/TiO_2 samples, i.e. $15\%MnO_x$-$5\%WO_3/TiO_2$ and $5\%WO_3/15MnO_x/TiO_2$,

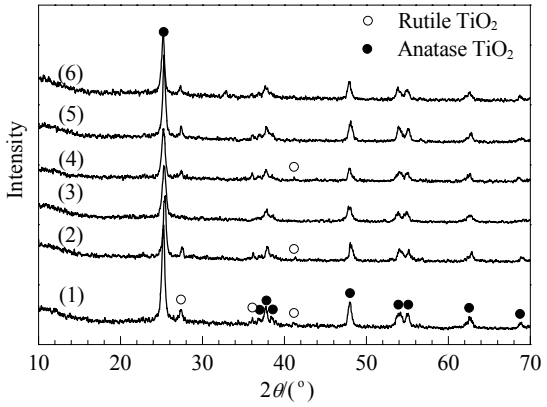

Fig. 1. XRD patterns of catalysts and supports. (1) TiO_2; (2) 15%MnO_x/TiO_2; (3) 15%MnO_x/5%WO_3/TiO_2; (4) 5%WO_3/15%MnO_x/TiO_2; (5) 5%WO_3/TiO_2; (6) 15%MnO_x-5%WO_3/TiO_2.

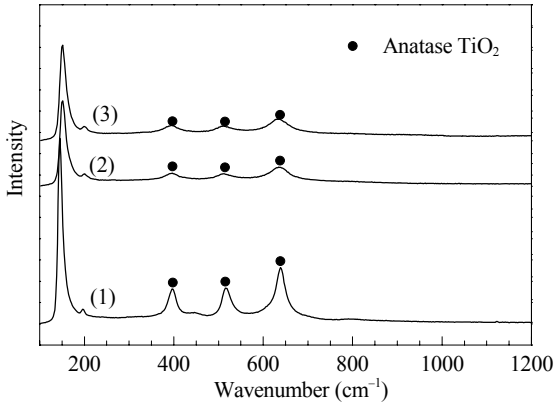

Fig. 2. LRS spectra of catalysts with TiO_2 as the reference of TiO_2 (1), 15%MnO_x/TiO_2 (2), and 15%MnO_x-5%WO_3/TiO_2 (3).

the XRD patterns were almost identical except that the weak peak corresponding to rutile TiO_2 (41.23°) had disappeared with the former while all other TiO_2 peaks were stronger than those of the latter sample. According to previous studies, the adding of WO_3 to TiO_2 can stabilize the crystal structure, thus preventing the transition from the anatase to rutile phase [29]. Hence, it was concluded that: (1) the disappearance of the rutile peaks was caused by the addition of WO_3, (2) the loading of tungsten prior to manganese gave the best dispersion of active components, indicating the strong interaction between the two metal oxides, and (3) the combination of WO_3 and MnO_x blocked the transformation from anatase to rutile.

For all the samples, no obvious peaks corresponding to MnO_x and WO_3 were observed, indicating that both metal oxides were highly dispersed on the surface.

2.3 LRS analysis

The comparison of the LRS spectra between the support and MnO_x/TiO_2 was shown in Fig. 2. It showed that after impregnating manganese oxide on the carrier, the peaks corresponding to anatase TiO_2 were much weakened but there was no appearance of manganese oxide, which was consistent with the XRD analysis. This indicated that Mn interacted with TiO_2 in the catalysts and covered the surface of TiO_2. There was no obvious change in the peak positions and intensities in the Raman spectra after adding 5% WO_3 into the MnO_x/TiO_2 catalysts (Figs. 2(2) and (3)).

2.4 Reduction properties of the catalysts

The catalytic activity of a SCR catalyst is closely related to its oxidation-reduction (redox) property, and a more facile redox property helps the transition of NO to NO_2, and thereby improves catalytic efficiency [30]. Figure 3 showed H_2-TPR spectra of the various catalysts modified with tungsten. The temperature at peak maximum and integrated peak areas showed that the reduction behavior of supported manganese catalysts mainly depends on the reducibility of the pure oxide support because the support oxide determines the reactivity of the bridging Mn–O–support functionality.

Figure 3 shows the H_2-TPR profiles of different catalyst. For the unmodified 15%MnO_x/TiO_2 catalyst, two reduction peaks at 325 and 419 °C were observed. Due to the extremely weak reducibility of WO_3 and TiO_2, these TPR peaks of the mixed oxides can be associated with the reduction of manganese oxide. The first peak, which was relatively weak but broad, probably corresponded to the reduction of $Mn_2O_3 \rightarrow Mn_3O_4$, while the latter was attributed to the reduction of $Mn_3O_4 \rightarrow MnO$ [31]. As reported by Li et al. and Kapteijn et al. [12], the MnO_x/TiO_2 catalyst prepared by the manganese acetate precursor had mainly Mn_2O_3 species [32]. After it was modified by tungsten oxide with the stepwise impregnation method, the first reduction peak of the

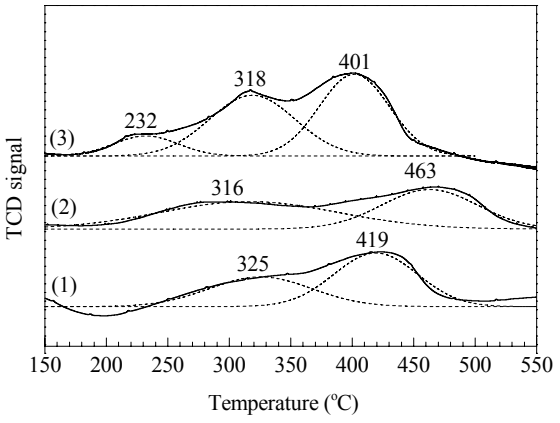

Fig. 3. H_2-TPR profiles of various catalysts. (1) 15%MnO_x/TiO_2; (2) 15%MnO_x/5%WO_3/ TiO_2; (3) 15%MnO_x-5%WO_3/TiO_2.

catalyst was shifted to a lower temperature and the peak area was increased, indicating that the addition of WO_3 improved the reducibility of the MnO_x/TiO_2 catalyst.

However, in the profile of the 15%MnO_x-5%WO_3/TiO_2 sample, the peak for dispersed MnO_x reduction was shifted to an even lower temperature after the addition of WO_3, and the first reduction peak at 325 °C was split into two peaks at 232 and 318 °C. In addition, the second peak at 419 °C had also shifted to a lower temperature (410 °C). These three peaks can be assigned to the stepwise reduction of surface dispersed MnO_x species, i.e., $Mn^{4+}\rightarrow Mn^{3+}\rightarrow Mn^{8/3+}\rightarrow Mn^{2+}$ [31]. The result suggested that the reduction behavior of MnO_x and oxidation state of Mn were affected by WO_3 addition.

In order to further understand the relationship between the preparation method of the Mn-based catalysts and the states of the Mn species, the peaks areas of the TPR profiles were integrated (shown in Table 2). The overlapping peaks were deconvoluted with Gaussian-Lorentz curves. From Table 2, it can be observed that the peak areas of the dispersed MnO_x species were increased after doping with WO_3. In particular, the 15%MnO_x-5%WO_3/TiO_2 sample exhibited the largest peak area of H_2 reduction and had the biggest H_2/Mn ratio, which clearly indicated that the manganese oxide was dispersed well. This can be explained by a nano-size effect. Smaller particles of mixed oxides have more exposed surface oxygen that readily reacted with hydrogen during reduction. Furthermore, it is also noteworthy that the H_2 consumption peak at 318 °C (from the reduction of $Mn^{4+}\rightarrow Mn^{3+}$) was larger than that of the peak at 232 °C (reduction of $Mn^{3+}\rightarrow Mn^{8/3+}$). This may be ascribed to the reduction of Mn_2O_3 to Mn_3O_4 occurring before the former was complete due to H_2 spillover, which has been reported elsewhere [33]. Hence, it was confirmed that the MnO_x on the surface was mainly Mn_2O_3 accompanied with some MnO_2.

Table 2 Peak information of the H_2-TPR results

Sample	Dispersed MnO_x			Total peak	I(peak I)/	(I(peak Ⅱ) + I(peak I))	H_2/Mn (mol/mol)			
	Peak I	Peak Ⅱ	Peak Ⅲ	area	I(peak Ⅱ)	/I(peak Ⅲ)	Peak I	Peak II	Peak III	Total
5%MnO_x/TiO_2	17.80	26.19	—	43.99	0.68	—	0.06	0.09	0.00	0.15
15%MnO_x/5%WO_3/TiO_2	28.81	22.31	—	51.12	1.29	—	0.10	0.08	0.00	0.17
15%MnO_x-5%WO_3/TiO_2	7.60	30.50	33.61	71.71	0.25	1.13	0.03	0.10	0.11	0.25

By comparing the ratio of the peak areas of Peaks I–III (shown in Table 2), for the unmodified sample, the reduction extent of Mn_2O_3 to Mn_3O_4 was lower than that of Mn_3O_4 to MnO. The reduction of Mn_2O_3 to Mn_3O_4 dominated the reduction process as for 15%MnO_x/5%WO_3/TiO_2. For the 15%MnO_x-5%WO_3/TiO_2 sample, the reductions of Mn_2O_3 to Mn_3O_4 and Mn_3O_4 to MnO were the main reduction processes. The ratio I(peak I)/I(peak II) or (I(peak I) + I(peak Ⅱ))/I(peak Ⅲ)) was in the sequence: 15%MnO_x/5%WO_3/TiO_2 > 15%MnO_x-5%WO_3/TiO_2 > 15%MnO_x/TiO_2. A higher ratio indicated a higher reducibility.

Taken together, the above analysis showed that the difference in reducibility reflected as peak maximum and peak area of these Mn-based mixed oxides depended strongly on the nature of the tungsten oxide employed. It was concluded that WO_3 greatly improved the reducibility of MnO_x-TiO_2 mixed oxides, especially in the low temperature window. From the positions of the H_2 reduction peaks and the areas, the 15%MnO_x-5%WO_3/TiO_2 sample had the most facile reducibility.

2.5 In situ FT-IR of NH_3 adsorption

To further investigate the influence of WO_3 addition and the various modification methods on the surface properties, in situ FT-IR analysis of NH_3 adsorption was employed. The results are shown in Fig. 4. The FT-IR spectra of ammonia adsorbed on acidic catalysts has been investigated extensively. The N–H deformation vibration of adsorbed ammonia, from 1000 to 1700 cm^{-1}, is an important fingerprint to differentiate the Lewis acid from Brönsted acid [34,35]. Alejandre et al. [36] reported that the band at 1600 cm^{-1} was associated with the asymmetric deformation vibration of ammonia adsorbed on a Lewis acid site, and the bands with

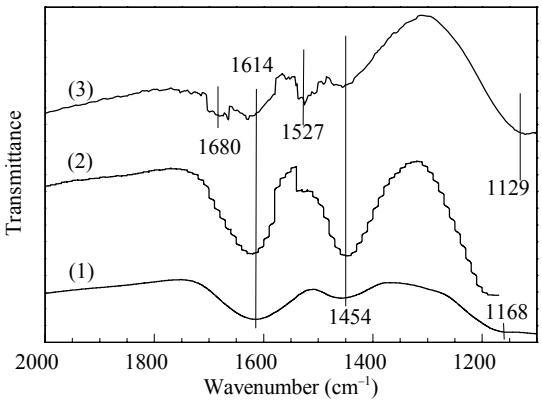

Fig. 4. NH_3 IR spectra of the three samples at 25 ºC. (1) 15% MnO_x/TiO_2; (2) 15%MnO_x5%WO_3/TiO_2; (3) 15%MnO_x/5%WO_3/TiO_2.

two split components at 1222 and 1155 cm^{-1} was due to the symmetric deformation of this type of adsorbed ammonia. On the other hand, many studies confirmed that the bands at 1450 and 1680 cm^{-1} arise from the asymmetric and symmetric deformation of NH_4^+ ($\delta_{as}(NH_4^+)$ and $\delta_s(NH_4^+)$) bound to Brönsted acid sites [36,37]. Therefore, Lewis acid and Brönsted acid sites existed on all the samples, as indicated by the bands at 1614, 1168, and 1129 cm^{-1} (Lewis acid sites), and 1680 and 1454 cm^{-1} (Brönsted acid sites). However, the number and size of the NH_3 adsorption peaks were different for the three samples.

For the MnO_x/TiO_2 sample, a stronger adsorption peak at 1614 cm^{-1} and weaker peaks at 1454 and 1168 cm^{-1} appeared, indicating that there were two kinds of Lewis acid sites and one kind of Brönsted acid sites.

For the sample prepared by the step-by-step impregnation, the peak at 1168 cm^{-1} was shifted to 1129 cm^{-1} and was slightly more intense, showing it had more Lewis acid sites. Meanwhile, the NH_3 adsorption peaks on 1614 and 1454 cm^{-1} sites were stable. It is worth noting that two new bands at 1680 and 1527 cm^{-1} appeared. The former at 1680 cm^{-1} was ascribed to NH_3 adsorption on Brönsted acid sites [38]. Ramis et al. [39] proposed that the band at 1535 cm^{-1} was due to amide species. Tsyganenko et al. [38] reported that a NH_2 deformation mode was observed in 1505–1580 cm^{-1}. Accordingly, the bands at 1527 cm^{-1} can be ascribed to the amide species. From the above analysis, it can be concluded that the addition of WO_3 increased considerably the surface acidity of the original mixed oxides, especially the Brönsted acidity, which was due to the strong Brönsted acidity of WO_3 [40]. Moreover, the WO_3 modified sample possessed more of the active intermediate species ($–NH_2$) for the NH_3 oxidation reaction.

Another WO_3-containing sample, i.e. the 15%MnO_x-5%WO_3/TiO_2 sample prepared by one-step impregnation, displayed an almost identical NH_3 spectra except that the peak area was larger, indicating that a larger amount of acid sites existed on the surface of the catalyst.

The above analysis showed that WO_3 doping drastically increased the surface acid sites of the MnO_x/TiO_2 samples, while the various loading methods of WO_3 affected the amount of acid sites on the surface.

For a further comparison of the acid sites on the catalysts, FT-IR results of ammonia adsorbed on the three samples at different temperatures were presented in Fig. 5. The presence of the adsorbed species at high temperatures was used to indicate the relative strength of the different acid sites. With increasing temperature, all the peaks associated with adsorbed ammonia on both Lewis acid sites and Brönsted acid sites gradually diminished until they had almost disappeared at 300 °C except for the peaks at 1680 and 1614 cm^{-1} from the WO_3-modified samples. This indicated coordinated ammonia was more thermally stable than ammonium ions on the tri-component catalysts.

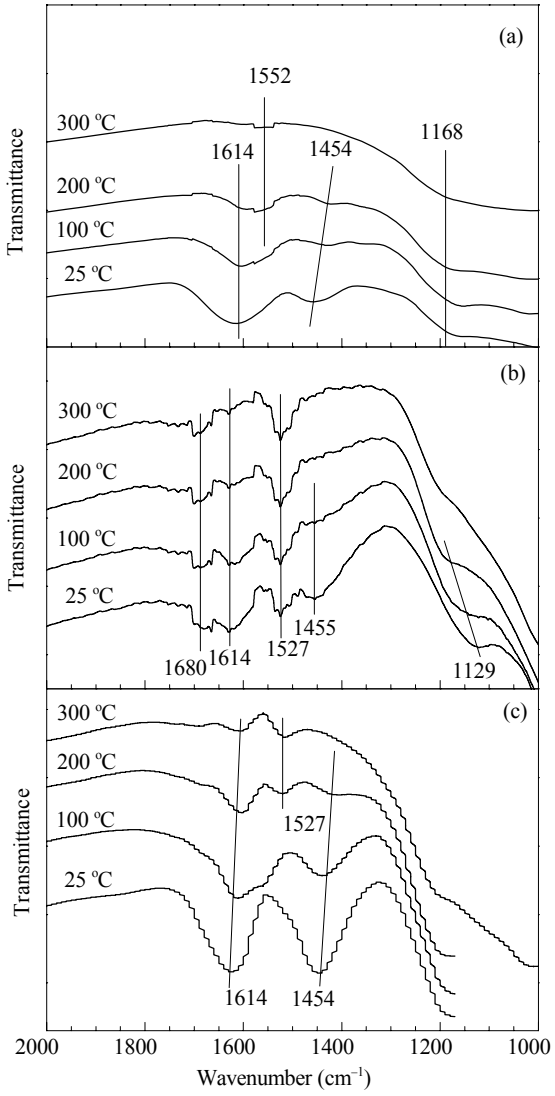

Fig. 5. FT-IR spectra of adsorbed NH_3 at different temperatures on 15%MnO_x/TiO_2 (a), 15%MnO_x/5%WO_3/TiO_2 (b), and 15%MnO_x-5%WO_3/TiO_2 (c).

A group of new peaks at 1552 cm^{-1} for the 15%MnO_x/TiO_2 sample and at 1527 cm^{-1} for the 15%MnO_x-5%WO_3/TiO_2 sample appeared and became stronger as the temperature increased. In addition, the group of weak peak at 1527 cm^{-1} for the 15%MnO_x/5%WO_3/TiO_2 sample also became stronger with the temperature increase. The peak at 1552 cm^{-1} was attributed to the intermediate species ($–NH_2$). With the increase of temperature, the peak intensity of $\delta_s(NH_3)$ declined gradually while that of the $–NH_2$ species increased, indicating that $–NH_2$ was formed from the decomposition of coordinated ammonia adsorbed on Lewis acid sites. Hence, it can be suggested that in addition to more surface acidity, the WO_3-modified catalysts also had

more active intermediates for the NH_3 oxidation reaction, which would be the reason for its higher catalytic activity.

2.6 HRTEM characterization

To understand the effect of the addition of WO_3 on the morphology and surface properties, HRTEM analysis was carried out on selected samples. Figure 6 showed HRTEM images from the catalysts prepared by the step-by-step impregnation and one-step impregnation. The catalysts were basically well dispersed spherical particles with the average diameter of 17 nm, which was in agreement with the XRD results. There was no real agglomeration of the particles, and there was just the trivial sectional agglomeration without distinct boundaries among the particles.

To determine the structure of these small particles, electron diffraction analysis was used. The results were shown in Fig. 7. The electron diffraction patterns indicated that MnO_x and WO_3 were both microscopic crystals. Compared with the images from the sample from the one-step impregnation, the images for the $15\%MnO_x/5\%WO_3/TiO_2$ sample had relatively clear and diffuse concentric circles with deepened halo, which indicated they were more polycrystalline and amorphous.

There was no big difference for the catalysts prepared with step-by-step or one-step impregnation in the HRTEM images. The catalyst obtained by one-step impregnation showed better dispersion than that from the step-by-step method.

2.7 Catalytic performance

Figure 8 showed that the optimum SCR activities of the catalysts were at 160–240 °C for all the samples. After adding 5% of WO_3 to the $15\%MnO_x/TiO_2$ catalyst, the catalytic activity exhibited different changes, which were determined by the impregnation sequence of the binary oxides, i.e., WO_3 and MnO_x, on the support. As shown in Fig. 8, when manganese was loaded before tungsten ($5\%WO_3/15\%MnO_x/TiO_2$), the catalytic activity displayed a declining trend in the whole temperature window (80–240 °C). The highest NO conversion rate dropped to 45% at 200 °C. For the other two kinds of WO_3-modified catalysts obtained by the one-step impregnation and step-by-step impregnation with prior addition of tungsten oxide, the NO conversion rates were enhanced. In the temperature range of 160–240 °C, the NO conversion rate was above 70%, indicating that the addition of WO_3 improved the catalytic activity of the MnO_x/TiO_2 catalyst. The improvement of catalytic performance was affected by the addition method of WO_3. The $15\%MnO_x$-$5\%WO_3/TiO_2$ sample gave the best catalytic performance with over 85% NO conversion rate in a wider

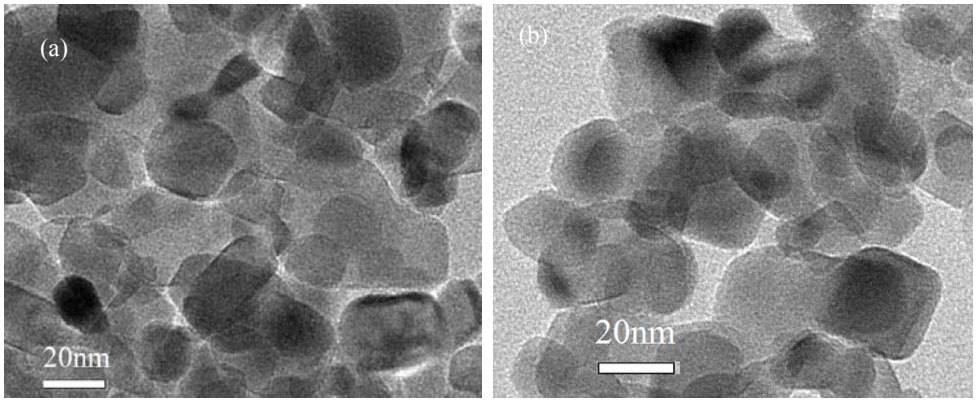

Fig. 6. HRTEM images of $15\%MnO_x/5\%WO_3/TiO_2$ (a) and $15\%MnO_x$-$5\%WO_3/TiO_2$ (b).

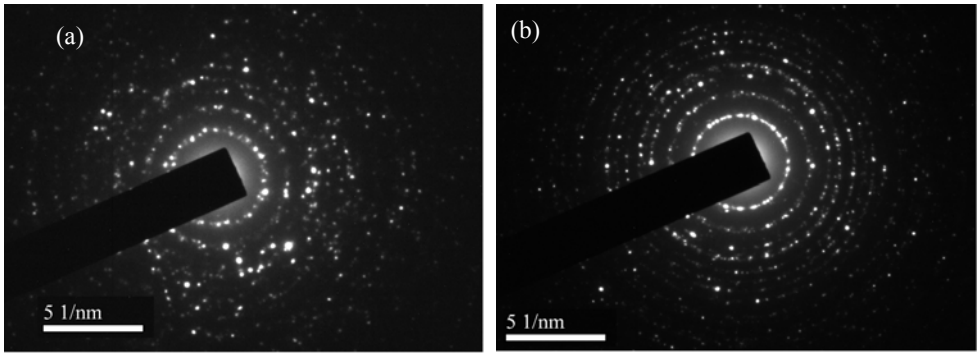

Fig. 7. Electron diffraction patterns of $15\%MnO_x/5\%WO_3/TiO_2$ (a) and $15\%MnO_x$-$5\%WO_3/TiO_2$ (b).

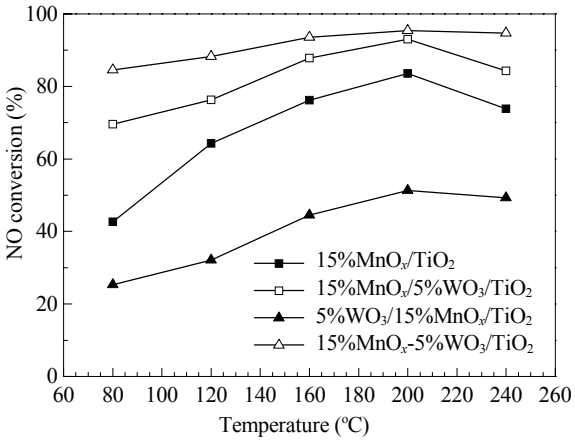

Fig. 8. NO conversion rates for the different catalysts.

temperature window (80–240 °C), which could be explained by the FT-IR analysis that the active sites for NH_3 adsorption were increased by WO_3 modification.

It is generally accepted that SCR activity is related to the surface acidity of the catalyst. However, Busca et al. [41] suggested that there is still some debate concerning the nature of the active sites and the active ammonia species. Some computational results indicated that the reaction occur on either Lewis acid or Brönsted acid sites, and the corresponding mechanism was proposed [42,43]. It is believed that Brönsted acid sites are not necessary for the reaction at low temperatures [11] while they are important for better catalytic activity for medium temperature SCR operation [44,45]. Zhu et al. [46] suggested that the activities at different temperatures were related to the acidity of the catalysts. They suggested that at low temperatures below 200 °C , weak Lewis acid sites were the main active sites, at medium temperature (~250–300 °C), Brönsted acid sites were the primary active sites, and at high temperatures (>350 °C), strong Lewis acid sites also promoted the reaction. Chen et al. [47] prepared a CeO_2-WO_3 catalyst that gave almost 100% NO conversion in the wide temperature range of 200–450 °C. They proposed that both NH^{4+} and coordinated NH_3 contributed to the SCR reaction.

The mechanism of the surface transformation of NO_x on Mn-based catalysts has been studied extensively. Qi et al. [30] proposed that the reaction of NH_2 and NO, and then the formation of nitrosamine (NH_2NO) is a typical SCR mechanism for V_2O_5/TiO_2 and manganese-based catalysts. Gaseous NO reacts with NH_2 to form a nitrosamine that decomposes into N_2 and H_2O. Kapteijn et al. [12] suggested that the interaction of NO, NH_3, and O_2 on manganese oxide can be explained by a model where NH_3 was successively dehydrogenated by surface oxygen. In this model, the intermediate ($–NH_2$) reacts with NO to form N_2, while (–NH) or (–N) species only react with NO to give N_2O. Kijlstra et al. [48] studied the mechanism of SCR of NO with ammonia at low temperatures on a MnO_x/Al_2O_3 catalyst. They reported that the reaction starts with the adsorption of NH_3 on Lewis acid, which was subsequently transforms into NH_2. NH_2 then reacts with gas phase NO (E-R mechanism) and nitrite intermediates on the surface (L-H mechanism).

From the FT-IR result on adsorbed NH_3, the WO_3-modified catalysts have a higher low temperature catalytic activity, which was due to their comparatively stable and considerate surface acidity and the formation of the active intermediate ($–NH_2$). Concerning the abundant Brönsted acid sites on WO_3/TiO_2 and its excellent high temperature catalytic activity [26], we can confirm that the Lewis acid sites played a major role in the low temperature catalytic reduction of NO_x while the Brönsted acid sites were important for the medium temperature reaction. In particular, the WO_3-doped samples synthesized by the one-step impregnation exhibited the best catalytic performance, which can be attributed to their slightly larger amount of Lewis acid sites (~1614 cm^{-1}). Therefore, we also concluded that the Lewis acid sites in the high wavenumber region were important for the low temperature SCR reaction.

There were other factors that contributed to the excellent performance of the 15%MnO_x-5%WO_3/TiO_2 sample. A larger specific surface area and low crystallinity were also important. Furthermore, the H_2-TPR results revealed that the 15%MnO_x-5%WO_3/TiO_2 sample possessed excellent reducibility. The results showed that the one-step impregantion was not only simpler, but also gave better low temperature catalytic acitivity.

3 Conclusions

The method of WO_3 addition, whether by stepwise or one-step impregnation, determined the structure, dispersion of active components, and redox properties and surface acidity of the ternary oxides. The 15%MnO_x-5%WO_3/TiO_2 and 15%MnO_x/5%WO_3/TiO_2 samples gave higher catalytic activity, with the former catalyst giving the best activity of above 85% NO conversion and a low take-off temperature at 80 °C. The characterization techniques revealed that a synergistic effect of tungsten and manganese oxides existed in the catalyst. XRD, HRTEM, and H_2-TPR results revealed that the 15%MnO_x-5%WO_3/TiO_2 sample was well dispersed and possessed a large specific surface area. The H_2-TPR analysis showed the existence of Mn_2O_3 on all the samples and the presence of a small amount of MnO_2 for 15%MnO_x-5%WO_3/TiO_2, which showed the best reducibility. In the WO_3-containing mixed oxides, MnO_x provided adsorption sites, while WO_3 increased the amount and strength of Brönsted acid sites and enhanced NO oxidation.

Both ionic NH^{4+} and coordinated NH_3 contribute to the SCR reaction, while Lewis acid sites and the active intermediate ($-NH_2$) had the major role.

References

1 Phil H H, Reddy M P, Kumar P A, Ju L K, Hyo J S. *Appl Catal B*, 2008, **78**: 301
2 Schneider H, Scharf U, Wokaun A, Baiker A. *J Catal*, 1994, **146**: 545
3 郭静, 李彩亭, 路培, 崔华飞, 彭敦亮, 文青波. 环境科学 (Guo J, Li C T, Lu P, Cui H F, Peng D L, Wen Q B. *Chin J Environ Sci*), 2011, **32**: 2240
4 侯亚芹, 黄张根, 马建蓉, 郭士杰. 催化学报 (Hou Y Q, Huang Zh G, Ma J R, Guo Sh J. *Chin J Catal*), 2009, **30**: 1007
5 Zhao Q S, Sun L S, Liu Y, Su S, Xiang J, Hu S. *J Central South Univ of Technol*, 2011, **18**: 1883
6 Ramis G, Yi L, Busca G, Turco M, Kotur E, Willey R J. *J Catal*, 1995, **157**: 523
7 Irfan M F, Qurashi A, Alam M W. *Arabian J Sci Eng*, 2010, **35**: 79
8 Fabrizioli P, Burgi T, Baiker A. *J Catal*, 2002, **206**: 143
9 Richter M, Trunschke A, Bentrup U, Brzezinka K W, Schreier E, Schneider M, Pohland M M, Fricke R. *J Catal*, 2002, **206**: 98
10 Morales M R, Barbero B P, Cadus L E. *Appl Catal B*, 2007, **74**: 1
11 Peña D A, Uphade B S, Smirniotis P G. *J Catal*, 2004, **221**: 421
12 Kapteijn F, Singoredjo L, Andreini A, Moulijn T A. *Appl Catal B*, 1994, **3**: 173
13 徐海涛, 金保昇, 张亚平, 孙克勤, 汪小蕾. 东南大学学报 (自然科学版)(Xu H T, Jin B Sh, Zhang Y P, Sun K Q, Wang X L. *J Southeast Univ* (*Nat Sci Ed*)), 2012, **42**: 463
14 Wu Z B, Jiang B Q, Liu Y, Zhao W R, Guan B H. *J Hazard Mater*, 2007, **145**: 488
15 Qi G S, Yang R T, Chang R. *Catal Lett*, 2003, **87**: 67
16 唐晓龙, 郝吉明, 易红宏, 宁平, 李俊华. 中国环境科学 (Tang X L, Hao J M, Yi H H, Ning P, Li J H. *Chin Environ Sci*), 2007, **27**: 845
17 Shen B X, Liu T, Zhao N, Ma J, Hao X C. *Adv Mater Res*, 2011, **383-390**: 1945
18 Chen Z H, Wang F R, Li H, Yang Q, Wang L F, Li X H. *Ind Eng Chem Res*, 2012, **51**: 202
19 Liu F D, He H, Ding Y, Zhang C B. *Appl Catal B*, 2009, **93**: 194
20 李雪辉, 李华, 高翔, 陈志航, 杨青, 王芙蓉, 王乐夫. 催化学报 (Li X H, Li H, Gao X, Chen Zh H, Yang Q, Wang F R, Wang L F. *Chin J Catal*), 2011, **32**: 477
21 Wu Z B, Jiang B Q, Liu Y. *Appl Catal B*, 2008, **79**: 347
22 陈志航, 李雪辉, 高翔, 江燕斌, 吕扬效, 王芙蓉, 王乐夫. 催化学报 (Chen Zh H, Li X H, Gao X, Jiang Y B, L Y X, Wang F R, W L F. *Chin J Catal*), 2009, **30**: 4
23 Wu B J, Liu X Q, Xiao P, Wang S G. *Chem Res Chin Univ*, 2008, **24**: 615
24 张亚平, 赵晓媛, 孙克勤, 沈凯, 徐海涛, 周长城. 东南大学学报 (自然科学版)(Zhang Y P, Zhao X Y, Sun K Q, Shen K, Xu H T, Zhou Ch Ch. *J Southeast Univ* (*Nat Sci Ed*)), 2011, **41**: 1030
25 Nova I, Lietti L, Tronconi E, Forzatti P. *Catal Today*, 2000, **60**: 73
26 Chen J P, Yang R T. *Appl Catal A*, 1992, **80**: 135.
27 张亚平, 汪小蕾, 孙克勤, 沈凯, 徐海涛, 周长城. 燃料化学学报 (Zhang Y P, Wang X L, Sun K Q, Shen K, Xu H T, Zhou Ch Ch. *J Fuel Chem Technol*), 2011, **39**: 782
28 Zhang Y P, Zhao X Y, Xu H T, Shen K, Zhou C C, Jin B S, Sun K Q. *J Colloid Interface Sci*, 2011, **361**: 212
29 Kenevey K, Morris M A, Cunningham J, Ferrand G. *Key Eng Mater*, 1996, **118-119**: 303
30 Qi G S, Yang R T, Chang R. *Appl Catal B*, 2004, **51**: 93
31 Wu Z B, Jiang B Q, Liu Y, Wang H Q, Jin R B. *Environ Sci Technol*, 2007, **41**: 5812
32 Li J H, Chen J J, Ke R, Luo C K, Hao J M. *Catal Commun*, 2007, **8**: 1896
33 Sun C Z, Zhu J, Lv Y Y, Qi L, Liu B, Gao F, Sun K Q, Dong L, Chen Y. *Appl Catal B*, 2011, **103**: 206
34 Naito N, Katada N, Niwa M. *J Phys Chem B*, 1999, **103**: 7206
35 Larrubia M A, Ramis G, Busca G. *Appl Catal B*, 2000, **27**: 145
36 Alejandre A G, Ramirez J, Busca G. *Langmuir*, 1998, **14**: 630
37 Lietti L, Ramis G, Berti F, Toledo G, Robba D, Busca G, Forzatti P. *Catal Today*, 1998, **42**: 101
38 Tsiganenko A A, Pozdnyakov D V, Filimonv V N. *J Mol Struct*, 1975, **29**: 299
39 Ramis G, Busca G, Bregani F, Forzatti P. *Appl Catal*, 1990, **64**: 259
40 Lietti L, Aemany J L, Forzatti P, Busca G, Ramis G, Giamello E, Bregani F. *Catal Today*, 1996, **29**: 143
41 Busca G, Lietti L, Ramis G, Berti F. *Appl Catal B*, 1998, **18**: 1
42 Kobayashi M, Miyoshi K. *Appl Catal B*, 2007, **72**: 253
43 Vittadini A, Casarin M, Selloni A. *J Phys Chem B*, 2005, **109**: 1652
44 Topsøe N Y, Topsøe H, Dumesic J A. *J Catal*, 1995, **151**: 226
45 Schneider H, Tschudin S, Schneider M, Wokaun A, Baiker A. *J Catal*, 1994, **147**: 5
46 Zhu J, Gao F, Dong L H, Yu W J, Qi L, Wang Z, Dong L, Chen Y. *Appl Catal B*, 2010, **95**: 144
47 陈亮, 李俊华, 葛茂发, 马磊, 常化振. 催化学报 (Chen L, Li J H, Ge M F, Ma L, Chang H Zh. *Chin J Catal*), 2011, **32**: 836
48 Kijlstra W S, Brands D S, Smit H I, Poels E K, Bliek A. *J Catal*, 1997, **171**: 219